6-11-2018

Proton Irradiation Effect on Thermoelectric Properties of Nanostructured N-Type Half-Heusler $Hf_{0.25}Zr_{0.75}NiSn_{0.99}Sb_{0.01}$

Karthik Chinnathambi
Boise State University

Brian J. Jaques
Boise State University

Proton irradiation effect on thermoelectric properties of nanostructured n-type half-Heusler $Hf_{0.25}Zr_{0.75}NiSn_{0.99}Sb_{0.01}$

Nicholas Kempf,[1] Chinnathambi Karthik,[2] Brian J. Jaques,[2] Jonathan Gigax,[3] Lin Shao,[3] Darryl P. Butt,[4] Ran He,[5] Dezhi Wang,[5] Zhifeng Ren,[5] and Yanliang Zhang[1,a)]

[1]*Department of Aerospace and Mechanical Engineering, University of Notre Dame, Notre Dame, Indiana 46556, USA*
[2]*Micron School of Materials Science and Engineering, Boise State University, Boise, Idaho 83725-2090, USA*
[3]*Department of Nuclear Engineering, Texas A&M University, College Station, Texas 77843-3128, USA*
[4]*College of Mines and Earth Sciences, University of Utah, Salt Lake City, Utah 84112, USA*
[5]*Department of Physics and the Texas Center for Superconductivity, University of Houston, Houston, Texas 77204, USA*

(Received 6 February 2018; accepted 25 May 2018; published online 13 June 2018)

Thermoelectric properties of nanostructured half-Heusler $Hf_{0.25}Zr_{0.75}NiSn_{0.99}Sb_{0.01}$ were characterized before and after 2.5 MeV proton irradiation. A unique high-sensitivity scanning thermal microprobe was used to simultaneously map the irradiation effect on thermal conductivity and Seebeck coefficient with spatial resolution less than 2 μm. The thermal conductivity profile along the depth from the irradiated surface shows excellent agreement with the irradiation-induced damage profile from simulation. The Seebeck coefficient was unaffected while both electrical and thermal conductivities decreased by 24%, resulting in no change in thermoelectric figure of merit *ZT*. Reductions in thermal and electrical conductivities are attributed to irradiation-induced defects that act as scattering sources for phonons and charge carriers. *Published by AIP Publishing.*
https://doi.org/10.1063/1.5025071

Thermoelectric materials have promising applications in environments with high radiation flux, such as those in nuclear power plants and in space. For instance, in-pile thermoelectric devices can generate electricity from thermal energy to enable self-powered sensors for *in-situ* monitoring of critical parameters of the nuclear reactor pressure vessel and nuclear fuel assembly. In dry storage casks, thermoelectric devices can be used to power wireless sensor networks to actively monitor temperature and weld stability without costly power and data cable installation.[1] In space, radioisotope thermoelectric generators can provide steady power for decades and have been used on Mars and on deep-space probes.[2] Thermoelectric material performance is determined by the thermoelectric figure of merit $ZT = \alpha^2\sigma T/(\kappa_e + \kappa_l)$, where α is the Seebeck coefficient, σ is the electrical conductivity, T is the absolute temperature, and κ_e and κ_l are the electronic and lattice components of thermal conductivity, respectively.

While there have been some studies of the irradiation effect on thermoelectric materials in nuclear reactors, most have been performed on long-established bulk materials such as germanium telluride, bismuth telluride, and lead telluride.[3–5] The combination of thermal and fast neutron irradiation at relatively low temperature (<200 °C) created point defects in these materials, resulting in reduced carrier mobility and lower *ZT*.

Nanostructured half-Heusler alloys are promising thermoelectric materials for nuclear applications due to their environmental friendliness, high-temperature mechanical and thermal stability, and increased *ZT* compared to their bulk counterparts.[6–9] In addition to significant *ZT* enhancement realized through nanostructuring, these materials have potentially improved radiation tolerance due to high-density nanostructures and grain boundaries.[7–18] Nevertheless, there have been no reports of the irradiation effect on state-of-the-art nanostructured thermoelectric materials.

Protons and other ions are often used as surrogates for neutrons as they offer relatively high damage rates and superior control over dose and energy without rendering the material radioactive. However, the depth of damage caused by ion irradiation is typically limited to a few hundreds of nanometers for heavy ions and up to several tens of microns for light ions like protons. Since the irradiated layer is so thin, surface-sensitive methods must be used to characterize material properties in the damaged region. Additionally, the damage profile from ion irradiation is not uniform within this thin layer. For light ions, damage in the leading region is relatively uniform but is followed by a peak near the end of the cascade where substantial damage accumulates.[19,20] To date, all ion irradiation studies on thermoelectric materials have implemented bulk property measurements which fail to uncover the damage profile in the thin irradiated region.[21–25] In this work, microscale thermal conductivity and Seebeck coefficient are mapped as a function of depth from the irradiated surface. The damage profile is compared to the irradiation-induced vacancy concentration calculated with Transport of Ions in Matter (TRIM) simulation.[26]

The effect of 2.5 MeV proton irradiation on nanostructured half-Heusler $Hf_{0.25}Zr_{0.75}NiSn_{0.99}Sb_{0.01}$ is reported herein. Thermal conductivity, electrical conductivity, and Seebeck coefficient were characterized before and after proton irradiation. A unique scanning thermal microprobe technique with unprecedented sensitivity[27,28] was used to simultaneously characterize thermal conductivity and

a)Email: yzhang45@nd.edu. Telephone: +1-5746316669.

Seebeck coefficient with $<2\,\mu$m spatial resolution. In conjunction, standard measurement techniques were used to characterize and corroborate the macro- and microscale thermoelectric properties before and after irradiation. X-ray diffraction (XRD) and transmission electron microscopy (TEM) were used to compare the microstructure before and after irradiation.

First, thermal diffusivity was measured by laser flash and room-temperature thermal conductivity was found to be 5.31 W/m·K for the non-irradiated sample. In preparation for irradiation, a 1 mm × 17 mm bar was cut from the disk and masks were used to block protons in selected regions of the bar. Samples were irradiated with 2.5 MeV protons to a fluence of 2×10^{16}/cm^2 with 100 nA current—an energy and dose intermediate of those reported in other proton irradiation studies on thermoelectric materials.[24,25] After irradiation, scanning thermal microscopy (SThM) was performed on both the irradiated and non-irradiated surfaces at the same time, eliminating uncertainties associated with measurements taken at different times due to potential surface oxidation and contamination. Figure 1 shows SThM results from the incident surface of the selectively irradiated sample. The irradiated regions show a 14% reduction in thermal conductivity compared with the non-irradiated regions. On the other hand, there is no statistically significant difference in the Seebeck coefficient between the irradiated and non-irradiated regions.

Next, the bar was cut and polished to expose a cross section containing both the irradiated region near the incident surface and the bulk, non-irradiated region. Figure 2 shows the SThM results mapping thermal conductivity and Seebeck coefficient as a function of depth from the irradiated surface along with the damage profile calculated using TRIM simulation.

There is a clear reduction of thermal conductivity in the damaged region to a depth of 40 μm, with the apparent peak in damage occurring at a depth of 34 μm—an excellent agreement with the damage profile calculated using TRIM. The profile of property change is a characteristic shape with two distinct regions: (1) a relatively uniform reduction in thermal conductivity up to 30 μm from the surface and (2) a sudden decrease in thermal conductivity from 31 to 34 μm. Beyond 35 μm, the thermal conductivity quickly recovers to the non-irradiated value as the irradiation damage decays to naught. Thermal conductivity decreased from 5.4 W/m·K in the non-irradiated region to 4.1 W/m·K in the irradiated region up to 30 μm deep. There is no statistically significant

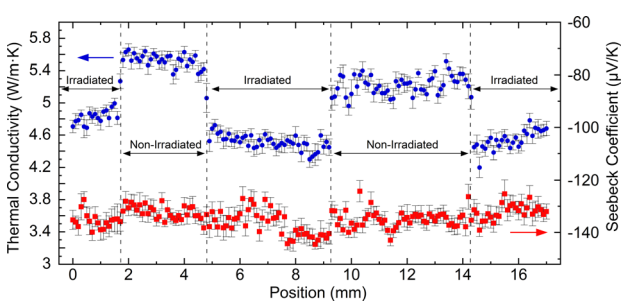

FIG. 1. Thermal conductivity and Seebeck coefficient of the selectively irradiated $Hf_{0.25}Zr_{0.75}NiSn_{0.99}Sb_{0.01}$ surface obtained using SThM. Dashed lines indicate boundaries between irradiated and non-irradiated regions.

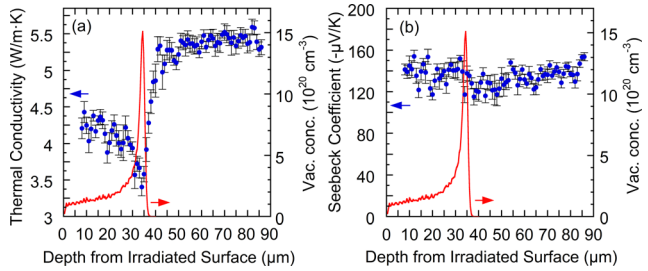

FIG. 2. (a) Thermal conductivity and (b) Seebeck coefficient as a function of depth from the irradiated surface of the $Hf_{0.25}Zr_{0.75}NiSn_{0.99}Sb_{0.01}$ sample obtained using SThM on the cross section of the irradiated bar. The red curve represents the concentration of irradiation-induced vacancies calculated using TRIM simulation assuming a displacement energy of 25 eV for each atom.[29] TRIM predicts 1 replacement collision for every 49 vacancies generated.

change in Seebeck coefficient, in agreement with the incident surface SThM results.

Based on the damage depth measured with SThM, a film of 35 μm thickness was prepared so that the entire depth of the film was irradiated. The bulk electrical conductivity and Seebeck coefficient of the film were measured before and after irradiation (shown in Fig. 3).

The decrease in electrical conductivity with increasing temperature is due to the high level of doping which renders the semiconducting nature of this material degenerate. Similarly, the increase in Seebeck coefficient with increasing temperature is characteristic of highly doped n-type half Heusler materials.[8,9,16] Electrical conductivity decreased by 24% at room temperature and 17% at 200 °C. The Seebeck coefficient changed negligibly at room temperature and increased by 1.5% at 200 °C; however, this small change is well within measurement uncertainty. This co-validates the Seebeck coefficient obtained from the incident surface and cross-sectional SThM.

XRD was performed on non-irradiated and irradiated sections of the selectively irradiated bar. Figure 4(a) shows no conspicuous difference between the diffraction patterns of irradiated and non-irradiated sections, indicating no detectable phase change due to the proton irradiation. Additionally, the diffraction patterns match closely with the cataloged phases, indicating excellent phase purity of the $Hf_{0.25}Zr_{0.75}NiSn_{0.99}Sb_{0.01}$ sample. However, when compared to those of the non-irradiated region, the two largest

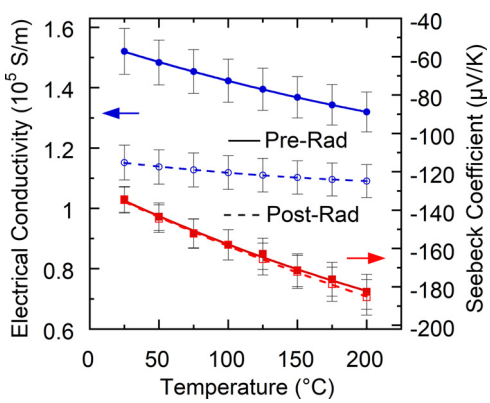

FIG. 3. Electrical conductivity and Seebeck coefficient of the $Hf_{0.25}Zr_{0.75}NiSn_{0.99}Sb_{0.01}$ film before and after proton irradiation.

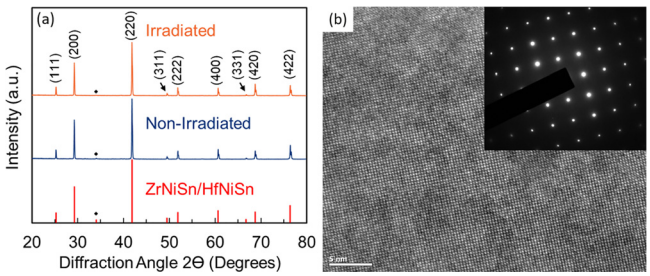

FIG. 4. (a) Results of XRD showing the diffraction pattern of irradiated (top/orange) and non-irradiated (middle/blue) $Hf_{0.25}Zr_{0.75}NiSn_{0.99}Sb_{0.01}$ along with the cataloged half-Heuslers (bottom/red). The small peak indicated by a diamond is associated with the half-Heusler phase, reported as unknown.[31] (b) High-resolution TEM image along the [001] zone axis of proton-irradiated $Hf_{0.25}Zr_{0.75}NiSn_{0.99}Sb_{0.01}$ with the inset showing the selected area electron diffraction (SAED) pattern.

diffraction peaks from the irradiated region show a 1.3% and 1.8% increase in full width at half maximum and a 14% and 18% decrease in integrated intensity at $2\theta = 29.3°$ and 41.8°, corresponding to (200) and (220), respectively. On the other hand, there is no measureable shift in the peak position. Considering that the XRD patterns were obtained sequentially from adjacent regions near the center of the selectively irradiated bar with no difference in grain size between regions, the peak broadening observed in the irradiated diffraction pattern indicates some degree of non-uniform microstrain not present in the non-irradiated region,[30] which is congruent with the theory that the proton irradiation generated point defects such as vacancies and interstitials.

TEM was performed on non-irradiated and irradiated specimens prepared from the same sample. Specimens were mechanically thinned to $<20\,\mu$m and then ion milled with Argon to <100 nm. The TEM images correspond to a depth of approximately 20 μm from the irradiated surface (in the nearly constant region of the damage profile). Figure 4(b) shows a typical high-resolution TEM image and selected area electron diffraction (SAED) pattern of an irradiated specimen. TEM images and SAED patterns before and after irradiation are fundamentally identical, revealing a high degree of crystallinity with no indication of local amorphization or transformation of the crystal structure, confirming that no extended defects were generated by the proton irradiation.

Seebeck coefficient is sensitive to the carrier concentration, as indicated by the expression for Seebeck coefficient in heavily doped semiconductors

$$\alpha = \frac{8\pi^2 k_B^2}{3eh^2} m^* T \left(\frac{\pi}{3n}\right)^{2/3}. \quad (1)$$

Here, k_B is Boltzmann's constant, e is the carrier charge, h is Planck's constant, m^* is the carrier effective mass, and n is the carrier concentration.[7,32] Since electrical conductivity decreased while Seebeck coefficient remained unchanged over the entire temperature range of measurement (Fig. 3), carrier mobility was markedly diminished by irradiation while changes in carrier concentration were insignificant.

To determine the relative influence of proton irradiation on lattice and electronic thermal conductivity, the Lorenz number was taken to be the Sommerfeld value. Using room temperature thermal conductivity from cross-section SThM, the electronic and lattice components of thermal conductivity were 1.11 and 4.25 W/m·K before irradiation, respectively. After irradiation, the values were 0.83 and 3.25 W/m·K, resulting in an ~24% reduction in both electronic and lattice thermal conductivity.

In an unlikely coincidence, the precise irradiation dose and energy resulted in nearly uniform mobility suppression of phonons and charge carriers in nanostructured $Hf_{0.25}Zr_{0.75}NiSn_{0.99}Sb_{0.01}$. Irradiation-induced point defects, such as vacancies, substantially reduce charge carrier mobility via local charge disorder.[33] At the same time, such defects create mass and strain fluctuations which scatter phonons and reduce the phonon mean free path.[34] While this nanostructured half-Heusler features nanograins which scatter long wavelength phonons,[8,35] the comparably high density of irradiation-induced point defects effectively suppresses phonons of shorter wavelength, further decreasing lattice thermal conductivity.

In summary, 2.5 MeV room temperature proton irradiation of nanostructured $Hf_{0.25}Zr_{0.75}NiSn_{0.99}Sb_{0.01}$ resulted in a 24% reduction in electrical and thermal conductivities with no change in Seebeck coefficient. The proton irradiation caused no extended defects but introduced point defects that act as scattering sources for phonons and charge carriers, lowering mobility. The combined effect of these property changes yielded no change in the thermoelectric figure of merit. Nevertheless, these property changes must be considered when using this material in radioactive environments, as the change in conductivities alters the material's *in-situ* thermal and electrical profiles.

This material is based upon work supported under an Integrated University Program Graduate Fellowship. This work was funded by the U.S. Department of Energy, Office of Nuclear Energy, under Award No. DE-NE0008255. N.K. acknowledges financial support from U.S. DOE NEUP fellowship support.

[1]D. A. Clayton, W. H. J. Andrews, and R. Lenarduzzi, ORNL, Report No. ORNL/TM-2012/442 (2012), p. 442.
[2]T. C. Holgate, R. Bennett, T. Hammel, T. Caillat, S. Keyser, and B. Sievers, J. Electron. Mater. **45**, 6044 (2016).
[3]J. C. Danko, G. R. Kilp, and P. V. Mitchell, Adv. Energy Convers. **2**, 79 (1962).
[4]J. Vandersande, J. McCormack, and A. Zoltan, *Intersociety Energy Conversion Engineering Conference* (1990), p. 392.
[5]M. Idnurm and K. Landecker, Br. J. Appl. Phys. **18**, 1209 (1967).
[6]Y. L. Zhang, M. Cleary, X. W. Wang, N. Kempf, L. Schoensee, J. Yang, G. Joshi, and L. Meda, Energy Convers. Manage. **105**, 946 (2015).
[7]S. Chen and Z. F. Ren, Mater. Today **16**, 387 (2013).
[8]S. Chen, K. C. Lukas, W. S. Liu, C. P. Opeil, G. Chen, and Z. F. Ren, Adv. Energy Mater. **3**, 1210 (2013).
[9]H. Zhang, Y. M. Wang, K. Dahal, J. Mao, L. H. Huang, Q. Y. Zhang, and Z. F. Ren, Acta Mater. **113**, 41 (2016).
[10]J. Yang, G. P. Meisner, and L. Chen, Appl. Phys. Lett. **85**, 1140 (2004).
[11]Y. T. Liu, H. H. Xie, C. G. Fu, G. J. Snyder, X. B. Zhao, and T. J. Zhu, J. Mater. Chem. A **3**, 22716 (2015).
[12]Q. Shen, L. Chen, T. Goto, T. Hirai, J. Yang, G. P. Meisner, and C. Uher, Appl. Phys. Lett. **79**, 4165 (2001).
[13]S. Sakurada and N. Shutoh, Appl. Phys. Lett. **86**, 082105 (2005).
[14]G. Joshi, T. Dahal, S. Chen, H. Z. Wang, J. Shiomi, G. Chen, and Z. F. Ren, Nano Energy **2**, 82 (2013).

[15]L. H. Huang, Q. Y. Zhang, B. Yuan, X. Lai, X. Yan, and Z. F. Ren, Mater. Res. Bull. **76**, 107 (2016).
[16]G. Joshi, X. Yan, H. Z. Wang, W. S. Liu, G. Chen, and Z. F. Ren, Adv. Energy Mater. **1**, 643 (2011).
[17]A. Bhardwaj, D. K. Misra, J. J. Pulikkotil, S. Auluck, A. Dhar, and R. C. Budhani, Appl. Phys. Lett. **101**, 133103 (2012).
[18]H. H. Xie, H. Wang, Y. Z. Pei, C. G. Fu, X. H. Liu, G. J. Snyder, X. B. Zhao, and T. J. Zhu, Adv. Funct. Mater. **23**, 5123 (2013).
[19]M. J. Swenson and J. P. Wharry, J. Nucl. Mater. **467**, 97 (2015).
[20]K. Nordlund, J. Keinonen, M. Ghaly, and R. S. Averback, Nature **398**, 49 (1999).
[21]G. S. Fu, L. Zuo, J. Lian, Y. Q. Wang, J. Chen, L. T. Jon, and Z. G. Xiao, Nucl. Instrum. Methods Phys. Res., Sect. B **358**, 229 (2015).
[22]T. Chang, J. Kim, M. J. Song, and W. Lee, AIP Adv. **5**, 057101 (2015).
[23]J. W. Roh, D. H. Ko, J. Kang, M. K. Lee, J. H. Lee, C. W. Lee, K. H. Lee, J. S. Noh, and W. Lee, Phys. Status Solidi A **210**, 1438 (2013).
[24]P. Chaudhari and M. B. Bever, J. Appl. Phys. **37**, 4181 (1966).
[25]A. Saji, S. Ampili, S. H. Yang, K. J. Ku, and M. Elizabeth, J. Phys.: Condens. Matter **17**, 2873 (2005).
[26]J. F. Ziegler, M. D. Ziegler, and J. P. Biersack, Nucl. Instrum. Methods Phys. Res., Sect. B **268**, 1818 (2010).
[27]N. Kempf and Y. Zhang, "A robust high-sensitivity scanning thermal probe for simultaneous microscale thermal and thermoelectric property mapping" (unpublished).
[28]Y. L. Zhang, C. L. Hapenciuc, E. E. Castillo, T. Borca-Tasciuc, R. J. Mehta, C. Karthik, and G. Ramanath, Appl. Phys. Lett. **96**, 062107 (2010).
[29]A. Y. Konobeyev, U. Fischer, Y. A. Korovin, and S. P. Simakov, Nucl. Energy Technol. **3**, 169 (2017).
[30]G. K. Williamson and W. H. Hall, Acta Metall. **1**, 22 (1953).
[31]R. V. Skolozdra, E. E. Starodynova, and Y. V. Stadnyk, Ukr. Fiz. Zh. **31**, 1258 (1986).
[32]G. J. Snyder and E. S. Toberer, Nat. Mater. **7**, 105 (2008).
[33]C. Uher, J. Yang, S. Hu, D. T. Morelli, and G. P. Meisner, Phys. Rev. B **59**, 8615 (1999).
[34]L. Andrea, G. Hug, and L. Chaput, J. Phys.: Condens. Matter **27**, 425401 (2015).
[35]A. N. Gandi and U. Schwingenschlogl, Phys. Chem. Chem. Phys. **18**, 14017 (2016).